

An Efficient and Recyclable Sn-Based Phosphotungstic Acid with Tunable Brønsted/Lewis Acidity for Selective Oxidation of Benzyl Alcohol

Yousheng Zhou,^a Xingyu Mei,^a Zhe Cai,^a Qing Wang,^a Jiahui Duanmu,^a Ouyang Kai,^a
Haijiang Zhang,^{*b} Xiujuan Tang^a and Xiaoxiang Han^{†*a}

^aDepartment of Applied Chemistry, Zhejiang Gongshang University, 310018 Hangzhou, China

^bJiangsu Key Laboratory of Regional Resource Exploitation and Medicinal Research,
Huaiyin Institute of Technology, 223003 Huaian, China

A series of metal ion (M = Sn²⁺, Fe³⁺, Ni²⁺, Co²⁺, Ag⁺, Cu²⁺) exchanged tungstophosphoric acid (H₃PW₁₂O₄₀; TPA) catalysts with tunable Brønsted/Lewis acidity were synthesized and exploited for the oxidation of benzyl alcohol (BzOH) to benzaldehyde (BzH) using hydrogen peroxide (H₂O₂) as oxidant. The structure of these M-TPA composite salts was also characterized by Fourier transform infrared spectroscopy (FTIR), X-ray diffraction (XRD), thermogravimetric analyses (TGA) and solid-state ³¹P nuclear magnetic resonance (NMR) probe molecule method. Among these M-TPAs, the Sn_{1/2}H₂PW₁₂O₄₀ catalyst, which presented strong Brønsted acidity, the synergistic effect of Brønsted/Lewis and pseudo-liquid characteristic property, exhibited excellent catalytic activity and durability with 98.2% of BzH selectivity and 95.1% of BzH yield. The optimal conditions for the oxidation of BzOH optimized by response surface methodology (RSM) were as follows: n(BzOH)/n(H₂O₂) = 1:1.25, catalyst amount of 5.5 wt.% to BzOH, water amount of 17 mL, 3.3 h of reaction time, and temperature 393 K. Moreover, further kinetic study confirmed that the reaction order was 2.64 and the activation energy was 21.75 kJ mol⁻¹.

Keywords: heteropolyacid, selective oxidation, Brønsted/Lewis acidity, process optimization

Introduction

Carbonyl compounds are one of the most important intermediates in the fine chemicals such as perfumes, dyestuffs, and agro-processing chemicals industry.¹ The sustained growth of population, as well as the exponential growth of their quality of life, and the demand for more environmentally friendly synthesis methods in chemicals has increased. Traditional methods to obtain carbonyl compounds have involved oxidation of alcohols which is based on the use of oxidants under the stoichiometric amounts, like K₂Cr₂O₇, KClO, KMnO₄, MnO₂, pyridinium chlorochromate (PCC) and so on. However, most of these reported systems suffer from economic and environmental problems for the phenomenon of large amounts of by-products, high reagent load and toxicity of the material.^{2,3} Currently, catalyst-oriented liquid-phase selective oxidation of alcohols as a simple, economical route to the synthesis of carbonyl compounds has attracted the attention of researchers. Many transition metals which

have been employed as catalysts in this reaction, such as Pd, Ru, Ag and Au, showed a nice selectivity and conversion.⁴⁻⁸ Inevitably, there were still some defects in these metal catalysts due to toxicity of metal and easy desorption from the carrier.

In recent years, a great deal of research works⁹⁻¹⁴ have been done on catalytic oxidation reaction. From the perspective of green chemistry, the oxidant, namely hydrogen peroxide (H₂O₂), shows the advantages of mild operating conditions, excellent reaction selectivity and clean for the environment, which is an ideal oxidant for alcohol selective oxidation.^{15,16} Hydrogen peroxide often requires catalysts to stimulate its excellent oxidizing power. Besides, the oxidation approach overcomes the disadvantages on the use of environmentally undesirable solvents. In particular, the catalyst system combining polyoxometalates (POMs) with H₂O₂ is an efficient, environmentally friendly and low-cost catalyst system for oxidation reaction.¹⁷⁻²⁶ The POMs especially for tungstophosphoric acid (TPA; H₃PW₁₂O₄₀) with Keggin-type structure, always show invertible and rapid multi-electron redox behavior under gentle conditions, hence, they have been widely used as acidic

*e-mail: Zhanghj7822@126.com; hxx74@126.com

oxidation catalysts for the oxidation of alcohol, olefin or alkane on homogeneous and heterogeneous systems.^{27,28} Nevertheless, bulk POM catalysts are detrimental to recycling and separation for their efficient solubility in most polar solvents. Furthermore, the molecular diffusion and mass transport are limited for their intrinsic low surface areas ($< 10 \text{ m}^2 \text{ g}^{-1}$). To solve these problems, POM catalysts modified by different methods were prepared and utilized. The structure and acidic property of these catalysts can be regulated by H^+ exchange of POMs with various metal ions to form metal transformed undissolved POMs salts^{23,29-36} or organic compound to form inorganic-organic hybrid materials,^{24,37-43} as well as dispersion on porous solid to form supported catalysts.⁴⁴⁻⁴⁸ For modified POMs, the types of exchangeable activation always have a tremendous impact on their acidic properties and tertiary structure of the POMs salts, leading to great effect on their catalytic activity. TPAs exchanged by metal ion (Cs^+ , K^+ , Na^+ , Ce^{3+} , Cu^{2+} , Mn^{2+} , etc.) and organic compound [1-methyl-3-propyl-3-sulfonate imidazole salt (MIMPS), pyridine propyl-3-sulfonic acid group (PPS), *N,N*-dimethyl benzylamine propyl sulfonate (DMBPS), glycine (Gly), etc.] show excellent catalytic performance in esterification, acetylation and oxidation reactions.²⁹⁻⁴³ These multifunctional TPA-based catalysts have not only good catalytic activities but also excellent temperature-resistant low-cost, environmentally-friendly, as well as good separation and recyclability. Experimental and theoretical studies have also illustrated the catalytic process causing a Brønsted-Lewis acid synergy, through inducing Lewis metal center into the Brønsted acidic TPA.

Herein, a series of metal ion-exchanged phosphotungstic acid (M-TPA) have been synthesized, the adopted metals included Sn^{2+} , Fe^{3+} , Ni^{2+} , Co^{2+} , Ag^+ and Cu^{2+} . The metal-modified TPA catalysts were characterized by Fourier transform infrared spectroscopy (FTIR), X-ray diffraction (XRD) and thermogravimetric analyses (TGA). Particularly, the acidic property was investigated by solid-state ^{31}P magic angle spinning nuclear magnetic resonance (MAS NMR) method.⁴⁹⁻⁵² On the basis of Box-Behnken design (BBD), the effects of different reaction parameters were optimized by response surface method (RSM) and the oxidation kinetic model was also established under optimal conditions.

Experimental

Catalyst preparation

All materials were purchased from Aladdin Company (Shanghai, China) and used without purification. The metal

ion-exchanged tungstophosphoric acid (TPA; $\text{H}_3\text{PW}_{12}\text{O}_{40}$) was prepared under the procedure described elsewhere.^{40,41} Based on the typical synthesis procedure, a solution was obtained by dissolving 5.76 g $\text{H}_3\text{PW}_{12}\text{O}_{40}$ (0.002 mol) and appropriate amount of SnCl_2 into 40 mL deionized water, followed by continuous stirring for about 12 h at 368 K. After removal of water, the obtained product was washed with diether and followed by drying under vacuum at 348 K for 12 h. Thus, a series of Sn metal ion-exchanged TPA samples were synthesized and expressed as $\text{Sn}_x\text{H}_{3-2x}\text{PW}_{12}\text{O}_{40}$ ($x = 1/2, 1, 3/2$; x means the molar ratio of Sn/TPA). For comparison, the other metal ion-exchanged TPA samples were prepared with similar method by varying metal nitrate with $M = \text{Fe}, \text{Ag}, \text{Cu}, \text{Co}$ and Ni .

Catalyst characterization

Spectral analysis using the conventional KBr pellet procedure was performed with aid of FTIR experiments on a Bruker IFS-28 spectrometer with resolution of 4 cm^{-1} over the range of $4000\text{-}400 \text{ cm}^{-1}$. Structure of sample was also studied by XRD (Bruker D8 ADVANCE X-ray diffractometer) using $\text{Cu K}\alpha$ radiation (0.15418 nm) at 40 kV and 20 mA. The TGA were performed by heating the catalyst from 298 to 873 K at a rate of 10 K min^{-1} in flowing N_2 by TG209 (NETISCH). Solid-state ^{31}P MAS NMR sample characterization was carried out with Bruker-Biospin Avance-III 500 spectrometer at 202.46 MHz. The ^{31}P chemical shifts referred to the 85% H_3PO_4 aqueous solution. The details of sample treatment were conducted according to the process of literature description.⁵³

Catalytic reaction

Under atmospheric conditions, the oxidation reaction was performed in a three-necked round bottom flask with a condenser. In a typical experiment, a mixture of substrate (0.05 mol benzyl alcohol and 0.1 mol 30% H_2O_2) and catalyst (0.27 g, 5 wt.%) in deionized water (20 mL) was placed in reactor at room temperature. Then the mixture was placed into an oil bath by mechanical stirring at 393 K for 3.0 h. After reaction, the mixture was cooled to room temperature, extracted with acetic ether, and rinsed with brine solution and water. The catalyst was filtered from the mixture, and washed with diethyl ether for reuse. Productions for reaction were analyzed by gas chromatography (Agilent 7890B GC; HP-5; $30 \text{ m} \times 0.25 \text{ mm} \times 0.25 \mu\text{m}$) with diphenyl as the internal standard. Catalytic properties of metal ion-exchanged TPAs catalysts were listed in Table 1 on the oxidation of BzOH with H_2O_2 .

Table 1. Catalytic activities of M-TPAs catalysts on the oxidation of BzOH with H₂O₂^a

Catalyst	BzOH conversion ^b / %	BzH selectivity ^b / %	BzH yield / %
H ₃ PW ₁₂ O ₄₀	62.31	93.52	58.27
SnCl ₂	5.39	99.67	5.37
Sn _{1/2} H ₂ PW ₁₂ O ₄₀	97.21	95.92	93.24
Sn ₁ HPW ₁₂ O ₄₀	89.51	95.33	85.33
Sn _{3/2} PW ₁₂ O ₄₀	68.14	95.66	65.18
Fe _{1/3} H ₂ PW ₁₂ O ₄₀	84.90	94.52	80.25
Co _{1/2} H ₂ PW ₁₂ O ₄₀	85.28	93.22	79.50
Ni _{1/2} HPW ₁₂ O ₄₀	92.52	95.69	88.53
Cu _{1/2} H ₂ PW ₁₂ O ₄₀	86.72	92.43	80.16
AgH ₂ PW ₁₂ O ₄₀	90.64	95.68	86.72

^aReaction conditions: 393 K, n(BzOH)/n(H₂O₂) = 1:2, 5 wt.% catalyst amount relative to BzOH, 4 h, 20 mL H₂O; ^banalyzed by GC.

Response surface methodology

Based on RSM, a series of experimental designs for the experimental factors were applied to optimize the production process of BzH by oxidation of BzOH with H₂O₂ over Sn_{1/2}H₂PW₁₂O₄₀. Four independent experimental variables, namely catalyst amount (x_1), BzOH/H₂O₂ mole ratio (x_2), water amount (x_3), and reaction time (x_4) were utilized by BBD. All factors were established and shown in Table 2, and coded into three levels (-1, 0, +1). Additionally, a 3⁴ full-factorial center composition designed with three coded levels was utilized, including 24 factorial and 5 central points, as listed in Table 3. The encoding values of these factors were derived from equation 1:

$$x_i = \frac{X_i - X_0}{\Delta X_i} \quad (1)$$

where ΔX_i represents the step-change value, while X_0 , x_i and X_i ($i = 1-3$) mean the central, coded, and real value of the various variables, respectively.

Utilizing the quadratic polynomial model equation given by RSM, the interactions between those variables

Table 2. Coded values and parameter levels used in the experimental design

Factor	Symbol	Range and level		
		-1	0	1
Catalyst amount / wt.%	x_1	4	5	6
BzOH/H ₂ O ₂ molar ratio / (mol mol ⁻¹)	x_2	1:1	1:2	1:3
Water amount / mL	x_3	15	20	25
Reaction time / h	x_4	3	4	5

were studied to make the course of reaction as effective as possible and forecast the product yield (i.e., BzH), which can be shown as:

$$Y = \beta_0 + \sum_{i=1}^4 \beta_i x_i + \sum_{i=1}^4 \beta_{ii} x_i^2 + \sum_{i < j}^4 \beta_{ij} x_i x_j \quad (2)$$

where β_0 , β_i , β_{ii} , and β_{ij} represent the regression coefficient of the variables, linear, quadratic, and interactive terms, respectively, while x_i and x_j ($i, j = 1-4$) denote the level of code for independent variables. The significance and effectiveness of the presented model were evaluated by statistic parameters on the basis of the analysis of variance (ANOVA) means.

Kinetic study

Oxidation kinetics under various conditions was studied by the initial reaction rate method, leading to the obtention of the kinetic expression. In this work, diverse experimental parameters were studied, such as BzOH/H₂O₂ mole ratio, temperature, and so on, while other parameters remained unchangeable. The reaction rate (r) may be indicated as:

$$r = -dC_A/dt = k' C_A^\alpha C_B^\beta \quad (3)$$

where C_A and C_B indicate the instant concentration of BzOH and H₂O₂, respectively; k' is the rate constant, α and β the reaction order corresponding to BzOH and H₂O₂.

Taking the natural logarithm, the above equation can be expressed as:

$$\ln r = \ln k + \alpha \ln C_A \quad (4)$$

where $k = k' C_B^\beta$ represents the modified parameter. Therefore, the rate constant was associated with the activation energy (E_a) by the Arrhenius equation:

$$\ln k = \ln k_0 - \frac{E_a}{R} \frac{1}{T} \quad (5)$$

where R is the gas constant, T the reaction temperature, and k_0 the pre-exponential factor.

Results and Discussion

Catalysts characterization

According to Figure S1 from the Supplementary Information section (hereinafter referred to as SI), FTIR spectra of original H₃PW₁₂O₄₀ and Sn_xH_{3-2x}PW₁₂O₄₀ ($x = 1/2, 1, 3/2$) samples were compared. Despite the reduction of

Table 3. Box-Behnken design (BBD) and response values

No. experiment	Variable and level				Yield / %	
	x_1	x_2	x_3	x_4	Experimental	Calculated
1	-1	-1	0	0	84.36	83.98
2	1	-1	0	0	88.53	88.97
3	-1	1	0	0	80.01	79.94
4	1	1	0	0	72.53	73.28
5	0	0	-1	-1	88.52	88.31
6	0	0	1	-1	82.71	83.58
7	0	0	-1	1	80.49	79.99
8	0	0	1	1	88.73	89.31
9	-1	0	0	-1	80.11	79.72
10	1	0	0	-1	88.53	88.34
11	-1	0	0	1	87.91	87.87
12	1	0	0	1	77.43	77.59
13	0	-1	-1	0	89.41	90.77
14	0	1	-1	0	74.07	73.86
15	0	-1	1	0	86.04	86.02
16	0	1	1	0	84.79	83.20
17	-1	0	-1	0	83.72	84.01
18	1	0	-1	0	84.29	83.56
19	-1	0	1	0	86.11	86.69
20	1	0	1	0	85.92	85.48
21	0	-1	0	-1	89.87	89.20
22	0	1	0	-1	75.31	75.90
23	0	-1	0	1	85.21	84.47
24	0	1	0	1	77.51	78.04
25	0	0	0	0	94.01	93.23
26	0	0	0	0	92.68	93.23
27	0	0	0	0	93.21	93.23
28	0	0	0	0	92.72	93.23
29	0	0	0	0	93.51	93.23

x_1 : catalyst amount; x_2 : BzOH/H₂O₂ molar ratio; x_3 : water amount; x_4 : reaction time.

peak strength and slight deviation of peak positions for Keggin structure, the four characteristic peaks at 1081, 981, 888 and 804 cm⁻¹ emerged obviously for all promoted samples, which was ascribed to stretching vibrations of PO_a and WO_d related with the central (O_a) and terminal (O_d) oxygens.^{49,51} Additionally, the absorption peaks at 517 and 597 cm⁻¹ were ascribed to the symmetric vibrations of W–O–W and O–P–O, respectively,³⁶ also revealing that all promoted catalysts kept the Keggin structure. Likewise, the reduction of band strength at 3427 cm⁻¹ ascribed to –OH (Figures S1b–S1d, SI section) implied that the acid protons of TPA were completely or partially displaced by Sn²⁺ cation. In this case, Sn²⁺ cation can exchange some or all protons in the H₅O₂⁺ form.⁵⁴

The phase purity of bulk samples was identified by powder X-ray analysis. The diffraction peaks of pure TPA and Sn_xH_{3–2x}PW₁₂O₄₀ series samples in Figure S2 (SI section) were consistent with available literature.⁵⁵

As exhibited in Figure S2b (SI section), the pure TPA displayed three main diffraction peaks of the Keggin polyanions structure at 2 θ degree of 10.3, 25.3 and 34.6°.⁵³ Predictably, the characteristic peaks were also presented in Sn_xH_{3–2x}PW₁₂O₄₀ series samples, and only the intensity of peaks reduced with the bonding of Sn (Figures S2c–S2e, SI section). On the other hand, the crystallinity of a series of catalysts was very similar to that of the parent TPA, which was consistent with previous reports.⁵⁵ However, the characteristic diffraction peak of SnCl₂ (Figure S2a, SI section) could not be identified, indicating the existence of a new metal modified TPA salt with fine crystallinity. Moreover, additional peaks related to the incorporated Sn²⁺ appeared in the 2 θ region of ca. 50–60°,³¹ which indicated the perfect anchoring of Sn²⁺ onto the TPA. The conclusions were consistent with FTIR results.

The thermal properties of pure H₃PW₁₂O₄₀ and metal exchanged TPAs were also determined by

TGA-DTG (derivative thermogravimetry) technique. Since $\text{Sn}_x\text{H}_{3-2x}\text{PW}_{12}\text{O}_{40}$ series catalysts presented similar TGA-DTG curves within the temperature range of 298-873 K, herein, only the curve for the $\text{Sn}_{1/2}\text{H}_2\text{PW}_{12}\text{O}_{40}$ sample was illustrated and discussed. As shown in Figure S3a (SI section), the pure SnCl_2 salt showed three major weight-loss peaks at 320, 420, and 720 K, which was ascribed to desorption of surface water, loss of crystal water, and partial decomposition of SnCl_2 , respectively. These results are distinct from the original TPA, which showed weight-loss peaks at 322, 470, and 663-788 K for the desorption of superficial water, loss of crystal water, and structural breakdown of Keggin frame, respectively.⁵⁶ By contrast, the $\text{Sn}_{1/2}\text{H}_2\text{PW}_{12}\text{O}_{40}$ sample exhibited similar weight-loss peaks to that of the original TPA at 321, 445 and 673-780 K (Figure S3c, SI section), in addition, there was a special existence of an extra weight-loss peak at 568 K, which may arise from the collapse of partial Keggin units formed in the existence of metal cations (Sn^{2+}). The thermal analysis results also indicated that metal cations (Sn^{2+}) were perfectly anchored with PW polyanions and kept steady at the temperature used for the catalytic studies.

In order to collect the acid properties information from samples, the ^{31}P -trimethylphosphine oxide (TMPO) MAS NMR could be employed to get the acid strength and the Brønsted or Lewis acid properties.^{49,50} It was evident that the observed ^{31}P NMR chemical shift ($\delta^{31}\text{P}$) of TMPO was facilitated by linear dependence with Brønsted acid strength.⁵² Actually, the original TPA adsorbed by TMPO typically exhibited multiple ^{31}P signals in two chemical shift scopes (Figure 1a). The sharp ^{31}P signals situated at -10 and -15 ppm can clearly arise from polyanions ($\text{PW}_{12}\text{O}_{40}^{3-}$) of the TPA, while those in the range of 55-95 ppm owing to Brønsted acid sites of the M-TPAs adsorbed by TMPO.^{40,41} It was remarkable that the original TPA had super acidic Brønsted acid sites (i.e., those with $\delta^{31}\text{P} \geq 86$ ppm),⁴⁹⁻⁵² as shown by the existence of ^{31}P resonance signals at 92, 88, and 83 ppm (Figure 1a) associated with three obtainable Brønsted H^+ sites adsorbed by TMPO (i.e., TMPOH^+). No resonance characteristics were observed for pure SnCl_2 adsorbed by TMPO (Figure 1e). Whereas the ^{31}P resonances was located within 55-80 ppm due to $(\text{TMPO})_n\text{H}^+$ ($n \geq 2$) species.⁵¹

Upon exchanging Sn^{2+} with the acidic protons (H^+) of TPA, similar resonance signals to original TPA were captured, nevertheless, the peaks emerged to be broadened (Figures 1b-1d). This also indicated that $\text{Sn}_x\text{H}_{3-2x}\text{PW}_{12}\text{O}_{40}$ ($x = 1/2, 1, 3/2$) catalysts maintained the Keggin structure of TPA and the local environments surrounding Brønsted acid sites, and the PW units may be changed with introducing Sn^{2+} into TPA. The strength and proportion

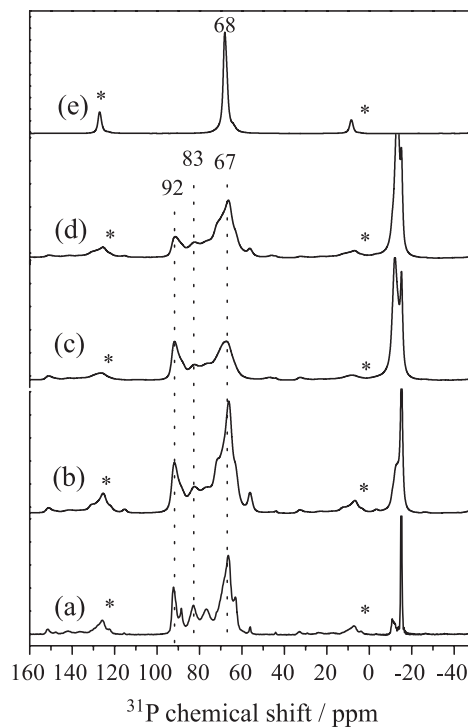


Figure 1. The ^{31}P NMR spectra (202.46 MHz) of sample adsorbed by TMPO with (a) pristine HPW ($\text{H}_3\text{PW}_{12}\text{O}_{40}$); (b) $\text{Sn}_{1/2}\text{H}_2\text{PW}_{12}\text{O}_{40}$; (c) $\text{Sn}_1\text{HPW}_{12}\text{O}_{40}$; (d) $\text{Sn}_{3/2}\text{PW}_{12}\text{O}_{40}$ and (e) SnCl_2 . Asterisks represent spinning sidebands.

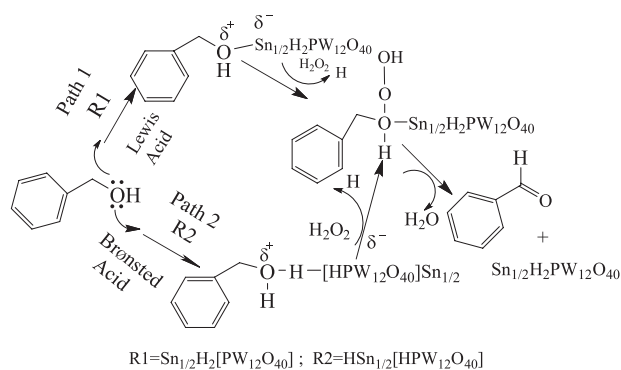
of resonance peaks of $\text{Sn}_x\text{H}_{3-2x}\text{PW}_{12}\text{O}_{40}$ ($x = 1/2, 1, 3/2$) catalysts, especially in the region of 89-95 ppm, decreased with increasing Sn loading. However, peak intensity at ca. 67 ppm increased with Sn loading increasing, implying the forming of Lewis acid sites.^{50,57} Unluckily, the peaks produced by $(\text{TMPO})_n\text{H}^+$ adducts ($n > 1.0$) were seriously overlaid with signals for Lewis acidity, which hindered the reasonable explanation for the change of acidity with Sn loading. Nevertheless, the acidic strength of various samples may be inferred following the descending order: $\text{H}_3\text{PW}_{12}\text{O}_{40} \gg \text{Sn}_{1/2}\text{H}_2\text{PW}_{12}\text{O}_{40} > \text{Sn}_1\text{HPW}_{12}\text{O}_{40} > \text{Sn}_{3/2}\text{PW}_{12}\text{O}_{40} \gg \text{SnCl}_2$.

Oxidation of benzyl alcohol to benzaldehyde

The acidic property of catalyst is related to its catalytic activity in some reaction catalyzed by acid. Oxidation of alcohol to aldehyde (ketone) using H_2O_2 as oxidant is a representative acid-catalyzed reaction. Strong acidic conditions can improve the oxidizability of H_2O_2 .⁵⁸ The catalytic activities of all metal ion-exchanged TPA and the original TPA were investigated during the oxidation of BzOH and the results were listed at Table 1. As listed in Table 1, SnCl_2 exhibited ignorable BzH yield and BzOH conversion. All the metal ion-exchanged TPA salts displayed acceptable catalytic properties comparing with

the original TPA with strongest Brønsted acidity. Among them, the $\text{Sn}_{1/2}\text{H}_2\text{PW}_{12}\text{O}_{40}$ sample showed the best BzH yield (93.24%) and excellent catalytic activity with an optimum BzOH conversion (97.21%). The experimental results also showed that both BzH yield and BzOH conversion decreased with increasing Sn^{2+} loading in $\text{Sn}_x\text{H}_{3-2x}\text{PW}_{12}\text{O}_{40}$ TPA salts. According to the above acidity characterization, the amount of Brønsted acidity decreased and the amount of Lewis acidity increased as the Sn^{2+} content in $\text{Sn}_x\text{H}_{3-2x}\text{PW}_{12}\text{O}_{40}$ samples increased. The purely Brønsted ($\text{H}_3\text{PW}_{12}\text{O}_{40}$) and solely Lewis ($\text{Sn}_{3/2}\text{PW}_{12}\text{O}_{40}$) samples showed inferior catalytic activities in contrast to the partially ion-exchanged TPA salts, which clearly indicated the synergistic influence of Brønsted-Lewis acid. More super-strong Brønsted acidity was not conducive to the oxidation of alcohols.

The synergy influence of Brønsted-Lewis acid can be attributed to the forceful ionic interactions among the Brønsted acidic proton (H^+), Lewis acidic metal ion (i.e., Sn^{2+}), and the $\text{PW}_{12}\text{O}_{40}^{3-}$ polyanion in ion-exchanged TPA salts.²⁹ A possible mechanism for BzOH oxidation to BzH over the M-TPAs was similar to the procedure described in literature.^{59,60} The oxidation of BzOH to BzH was catalyzed by Lewis acid (path 1) and Brønsted acid (path 2) based on the structural characteristics and afore discussed acidity characterization of the $\text{Sn}_{1/2}\text{H}_2\text{PW}_{12}\text{O}_{40}$ catalyst (Scheme 1). The catalytic performance of the catalyst was mainly related to the ratio of Brønsted acid to Lewis acid (B/L ratio) in the catalyst. In the cards, H_2O_2 first underwent the elimination of the β -hydride and then combined with the carbonyl group to form the final products BzH and water. Based on previous results, the conclusion of synergy effect of Brønsted-Lewis acid was put forward. Apart from the synergy influence of Brønsted-Lewis acid, the pseudo-liquid character of TPA and strong acidity were also responsible for excellent catalytic properties on the oxidation of BzOH over $\text{Sn}_{1/2}\text{H}_2\text{PW}_{12}\text{O}_{40}$ catalyst.



Scheme 1. Illustrative possible reaction mechanism for oxidation of BzOH over $\text{Sn}_{1/2}\text{H}_2\text{PW}_{12}\text{O}_{40}$ catalyst.

Process optimization

Since $\text{Sn}_{1/2}\text{H}_2\text{PW}_{12}\text{O}_{40}$ catalyst exhibited optimal catalytic properties among different Brønsted-Lewis M-TPA salts, it was selected for further process optimization. Owing to the improved efficacy, the impact from parameters like catalyst amount, BzOH/ H_2O_2 mole ratio, time of the reaction and water amount was investigated. As is well-known, the catalyst amount always played an important role in this selectivity oxidation.^{14,61} The effect of catalyst amount on the catalytic performance of BzOH oxidation with H_2O_2 was listed in Figure 2a. The conversion of BzOH almost linearly improved from 72.14 to 98.32% with the catalyst amount increasing to 6 wt.%. It was related to the gradual increase of active acid sites for catalytic oxidation. At the catalyst amount of 5 wt.%, a maximum yield of BzH (93.24%) was obtained. However, the BzH yield reduced significantly with further increasing the amount of catalyst, which was due to the decomposition of H_2O_2 resulted by the excessive amount of acid sites presented in the reaction system.^{14,29} Excess catalyst amount easily led to unsatisfactory oxidation of BzH and other reactions.

Also, the role of BzOH/ H_2O_2 mole ratio was investigated while other experimental variables kept constant, and the results were displayed in Figure 2b. Clearly, the BzH yield improved with BzOH/ H_2O_2 mole ratio increasing. The highest yield of BzH obtained was 93.24% with BzOH/ H_2O_2 mole ratio of 1:2 in 4 h. This implied that appropriate amount of H_2O_2 oxidant facilitated driving reaction equilibrium to form BzH. Nevertheless, further increase of BzOH/ H_2O_2 mole ratio led to a decrease of BzH yield probably due to the reactant (BzOH) and catalyst were too diluted, and the concentration of active center decreased with an excess of H_2O_2 . Meanwhile, excessive amount of H_2O_2 also provoked formation of undesirable oxidation of BzH, and thus, reducing BzH yield.

The influence of reaction time on BzH yield and BzOH conversion over the $\text{Sn}_{1/2}\text{H}_2\text{PW}_{12}\text{O}_{40}$ catalyst was studied at the range of 1-5 h with the conditions of catalyst amount = 5 wt.%, BzOH/ H_2O_2 mole ratio = 1:2, water amount = 20 mL, and reaction temperature = 393 K. As exhibited in Figure 2c, both BzH yield and BzOH conversion improved obviously at prolonged reaction time, reaching an excellent BzH yield (93.24%) at 4 h. Further increasing of reaction time caused a gradual decline in BzH yield, which may arise from the consumption of BzOH and the excess of BzH occupying the catalytic activity sites, hence, the oxidation of BzH of reaction improved with increasing reaction time and reduced BzH yield. Therefore, 4 h was chosen as reaction time for further study.

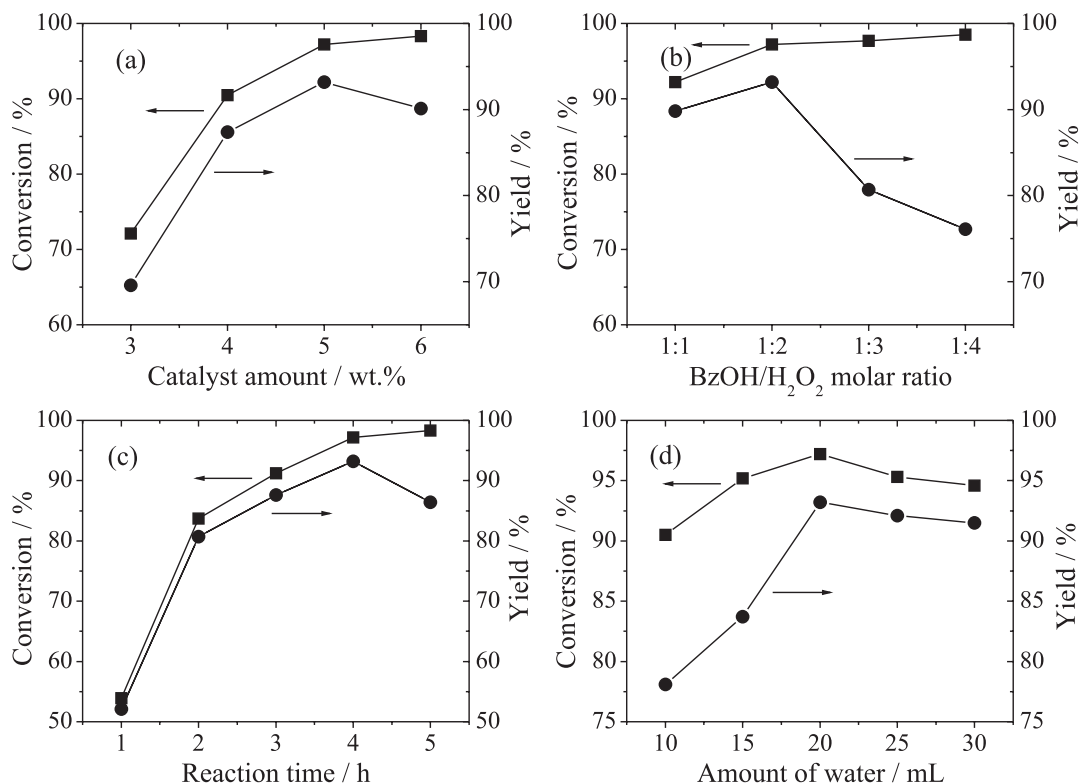


Figure 2. The conversion (■) and yield (●) of single experimental factor on the oxidation of BzOH with H₂O₂ over the Sn_{1/2}H₂PW₁₂O₄₀ catalyst: (a) catalyst amount; (b) BzOH/H₂O₂ molar ratio; (c) reaction time; (d) water amount.

Figure 2d depicted the influence of water amount on the selective oxidation of BzOH to BzH. Obviously, both BzH yield and original BzOH conversion improved with the amount of water increasing, reaching a maximum at 20 mL water, then descending gradually afterward. During alcohol oxidation reaction, the presence of water can easily form special droplets and was conducive to the adsorption and/or activation of molecular oxygen.^{8,62} Meanwhile, the existence of surface water can also enhance the oxygen mobility on catalyst to improve the number of oxygen vacant sites.^{63,64} However, the reaction system was diluted by excess water, and the available acid moiety of catalyst decreased. Based on the above experimental results, the best catalytic oxidation activities can be obtained under the optimum experimental conditions: $n(\text{BzOH})/n(\text{H}_2\text{O}_2) = 1:2$, 5 wt.% catalyst amount relative to BzOH, 4 h, 20 mL H₂O and 393 K.

Process optimization and model analysis

To optimize the reaction conditions of benzaldehyde (BzH) yield and assess interactions between experimental variable pairs, the factor-designed experiments and RSM were used. Table 3 listed the results of 29 experimental runs and the response values. By means of multiple regression analysis, using Design-Expert 6.0.5 software,⁶⁵ the response

Y (i.e., BzH yield), which may be related to independent experimental parameters by a quadratic model based on equation 2, can be indicated as:

$$Y = 93.23 - 0.42x_1 - 4.93x_2 + 1.15x_3 - 0.65x_4 - 5.10x_1^2 - 6.58x_2^2 - 3.18x_3^2 - 4.74x_4^2 - 2.91x_1x_2 - 0.19x_1x_3 - 4.72x_1x_4 + 3.52x_2x_3 + 1.72x_2x_4 + 3.51x_3x_4 \quad (6)$$

where the coded values x_1 , x_2 , x_3 and x_4 are catalyst amount, BzOH/H₂O₂ mole ratio, water amount, and reaction time, respectively. From regression of equation 6, a value of 0.9891 was obtained for coefficient of determination (R^2), exactly confirming that the model was credible and well fitted for experimental and predicted values.

Moreover, the standard ANOVA was used to determine if the quadratic model was sufficient and fitted the data, and the conclusions were listed in Table 4. From Table 4, the F -value of model for BzH yield was much larger than the tabular F -value for the 5% significance level. The F -value of 90.64 implied that the model was significant, and less than 0.0001 at 5% confidence level for P -value meant that the model was very significant. In this case, the significant model terms, x_2 , x_3 and x_4 , showing a low P -value at 5% confidence level, demonstrated that these variables were significant. The value of Pred R-Squared (0.9424) was consistent with the Adj R-Squared of 0.9782, definitely

implying that the model was of great significance. Besides, coefficient of variation (CV) was 1.04%, together with lack of fit F -value (3.11), implying that the model was more accurate. The experimental design was credible and there was less noise ratio and pure error.

The analysis chart was drawn according to the regression line equation, and the obtained two-dimensional (2D) contour plots together with three-dimensional (3D) response surface plots obtained were shown in Figures S4 and S5 (SI section), respectively. The contour plots visually reflected the effect of the interaction of various variables. The circle indicated that the interactive effect between two variables was not significant, and the ellipse indicates that the interaction was significant on these two factors. Therefore, from the Figures S4a and S5a (SI section), it can be observed that the interaction of x_1x_2 was significant, and similarly, the interactions of x_1x_4 , x_2x_3 , x_2x_4 , x_3x_4 were significant.

Combined with the mathematical analysis of the regression model, the optimal process parameters for oxidation of BzOH over the $\text{Sn}_{1/2}\text{H}_2\text{PW}_{12}\text{O}_{40}$ catalyst were obtained with amount of catalyst (x_1) = 5.49 wt.%, BzOH/ H_2O_2 mole ratio (x_2) = 1:1.26 mol mol⁻¹, water amount (x_3) = 16.95 mL and reaction time (x_4) = 3.33 h. Three parallel experimental runs were conducted to verify

the validity of the model under the optimum condition, and the average BzH yield was 95.1% with x_1 = 5.5 wt.%, x_2 = 1:1.25 mol mol⁻¹, x_3 = 17 mL, and x_4 = 3.3 h. The results were in good agreement with predicted value (95.6%). Therefore, the regression model was deemed with effectiveness and accuracy in predicting BzH yield.

Catalyst recycling

For reducing the experiment cost, the stability and recyclability of $\text{Sn}_{1/2}\text{H}_2\text{PW}_{12}\text{O}_{40}$ catalyst were investigated for the oxidation of alcohol. The tests were performed under above optimal conditions and the results were shown in Figure 3. The $\text{Sn}_{1/2}\text{H}_2\text{PW}_{12}\text{O}_{40}$ catalyst was mainly deposited in the lowest layer of the component after the reaction, which made the catalyst better reused by simple filtration due to the low solubility of the catalyst in the reaction system. After the leach of catalyst from the system for each cycle, it was washed by ethyl ether and dried under vacuum at 353 K for 12 h. As displayed in Figure 3, the $\text{Sn}_{1/2}\text{H}_2\text{PW}_{12}\text{O}_{40}$ catalyst exhibited good recyclability and stability after six consecutive experimental cycles. The BzOH conversion and BzH yield declined marginally from 99.1 and 95.1% of the first run to 94.9 and 92.8% after six consecutive running cycles, respectively. Additionally, the

Table 4. ANOVA data for the predicted BzH yield using the recommended quadratic model

Source	Sum of squares	DF	Mean square	F -value	Prob > F	Significance
Model	993.58	14	70.97	90.64	< 0.0001	a
x_1	2.08	1	2.08	2.65	0.1258	
x_2	292.05	1	292.05	372.99	< 0.0001	a
x_3	15.87	1	15.87	20.27	0.0005	b
x_4	5.03	1	5.03	6.43	0.0238	b
x_1^2	168.91	1	168.91	215.72	< 0.0001	a
x_2^2	280.78	1	280.78	358.59	< 0.0001	a
x_3^2	65.77	1	65.77	84.00	< 0.0001	a
x_4^2	145.92	1	145.92	186.36	< 0.0001	a
x_1x_2	33.93	1	33.93	43.33	< 0.0001	a
x_1x_3	0.14	1	0.14	0.18	0.6741	b
x_1x_4	89.30	1	89.30	114.05	< 0.0001	a
x_2x_3	49.63	1	49.63	63.39	< 0.0001	a
x_2x_4	11.76	1	11.76	15.03	0.0017	b
x_3x_4	49.35	1	49.35	63.03	< 0.0001	b
Residual	10.96	14	0.78			
Lack of fit	9.71	10	0.97	3.11	0.1428	
Pure error	1.25	4	0.31			
Cor total	1004.55	28				

^aHighly significant; ^bsignificant. DF: degrees of freedom; x_1 : catalyst amount; x_2 : BzOH/ H_2O_2 molar ratio; x_3 : water amount; x_4 : reaction time; Cor total: corrected total sum of squares.

FTIR measurements exhibited that the spent $\text{Sn}_{1/2}\text{H}_2\text{PW}_{12}\text{O}_{40}$ catalyst still had the integrity structure even after six continuous runs. The gradual decrease in BzOH conversion and BzH yield obtained after repeated runs arose from the leaching of TPAs in the process of regeneration. According to the elemental analyses by an inductively coupled plasma optical emission spectrometer (ICP OES) charge injection device (CID) detector (ICAP 6500; Thermo Scientific), the concentration of P in $\text{Sn}_{1/2}\text{H}_2\text{PW}_{12}\text{O}_{40}$ catalyst declined from 1.05 (fresh catalyst) to 0.91 wt.% after the fifth run, while the concentration of Sn element remained essentially unchanged. The above results indicated that the $\text{Sn}_{1/2}\text{H}_2\text{PW}_{12}\text{O}_{40}$ catalyst was not only durable but also recyclable for the alcohol oxidation reaction.

Kinetic model

The kinetic model for BzOH oxidation to BzH by H_2O_2 over the $\text{Sn}_{1/2}\text{H}_2\text{PW}_{12}\text{O}_{40}$ was established under

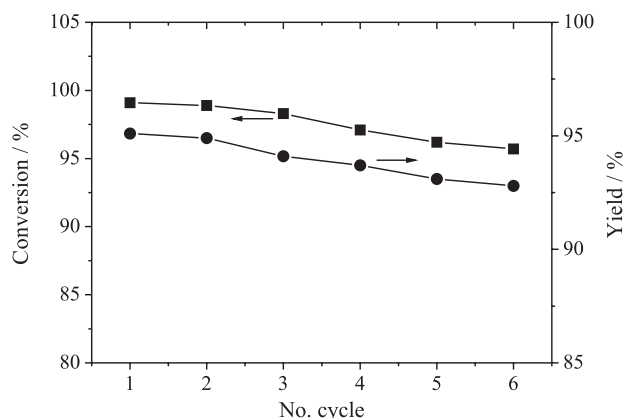


Figure 3. Stability of the $\text{Sn}_{1/2}\text{H}_2\text{PW}_{12}\text{O}_{40}$ catalyst on BzH yield (●) and BzOH conversion (■) during the oxidation of BzOH to BzH under optimal conditions.

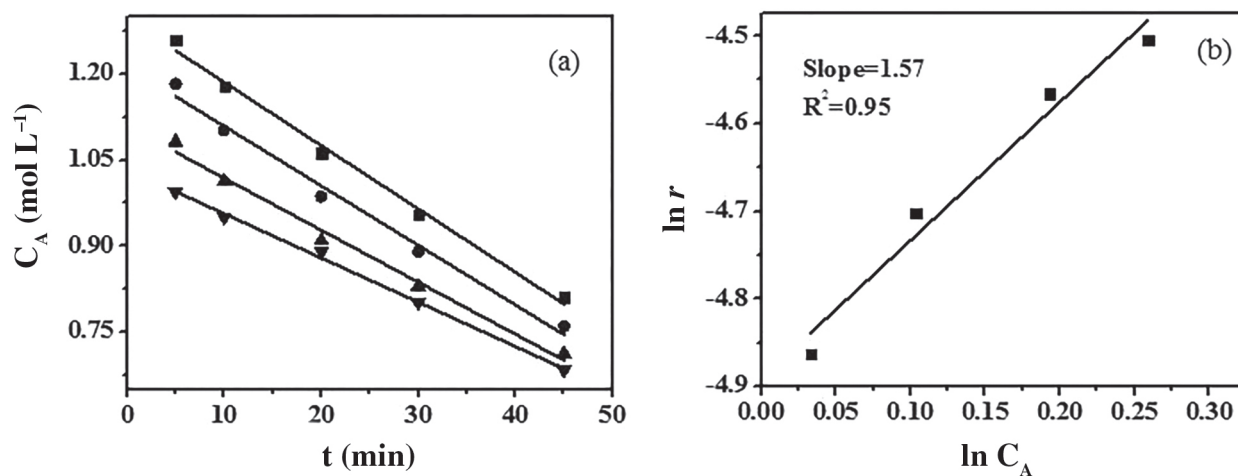


Figure 4. (a) Changes of BzOH concentration (C_A) vs. time and (b) log-log plot of primary oxidation rate vs. initial C_A . Symbols for initial C_A values: (■) 1.67, (●) 1.47, (▲) 1.27, and (▼) 1.11 mol L⁻¹. Reaction conditions: catalyst amount, 9.90 g L⁻¹; BzH concentration, 0 mol L⁻¹; initial H_2O_2 concentration, 2.18 mol L⁻¹; temperature, 393 K.

above optimum reaction conditions. The experiments were conducted at various reaction temperatures with different time. The reactant order of (BzOH; denoted as α) and oxidant (H_2O_2 ; denoted as β) had already been defined in equations 3 and 4. To correlate reaction rate with reactant concentration, the changes in concentration *versus* time were indispensable. In order to obtain the reaction order of BzOH (α), the reaction was carried out by changing the concentration of BzOH while keeping its corresponding constant. A set of parallel experiments were conducted under the initial amount of benzyl alcohol varying from 5.4 (0.050 mol) to 3.6 g (0.033 mol) and the time changing from 5 to 45 min. By fitting the data of each point, four fitted lines were obtained, the slope was the reaction rate (r), and the intercept was the initial concentration. According to equation 4, the logarithmic curves of concentration and reaction rate were derived in Figure 4b. The reaction order of BzOH ($\alpha = 1.57$) was obtained. Similarly, the linear decline of the H_2O_2 concentrations over time was shown in Figure 5a. The reaction rate and concentration of H_2O_2 were shown in Figure 5b and the reaction order of H_2O_2 was 1.07.

Also, the pre-exponential factor (k_0) of the reaction and activation energy (E_a) were defined in equation 5. To obtain the pre-exponential factor k_0 and activation energy E_a , the optimal reaction conditions were carried out under 5.5 wt.% of catalyst amount, 1:1.25 mol mol⁻¹ of $n(\text{BzOH})/n(\text{H}_2\text{O}_2)$, 17 mL of water, and 3.3 h for reaction with the temperature changing from 363 to 393 K (see Figure 6a). According to the temperature based on rate equation, the plots of $\ln k$ vs. $1/T$ were obtained by associating with equation 5 (Figures 6a and 6b). An activation energy $E_a = 21.75$ kJ mol⁻¹ was obtained. The value was slightly lower than that catalyzed by

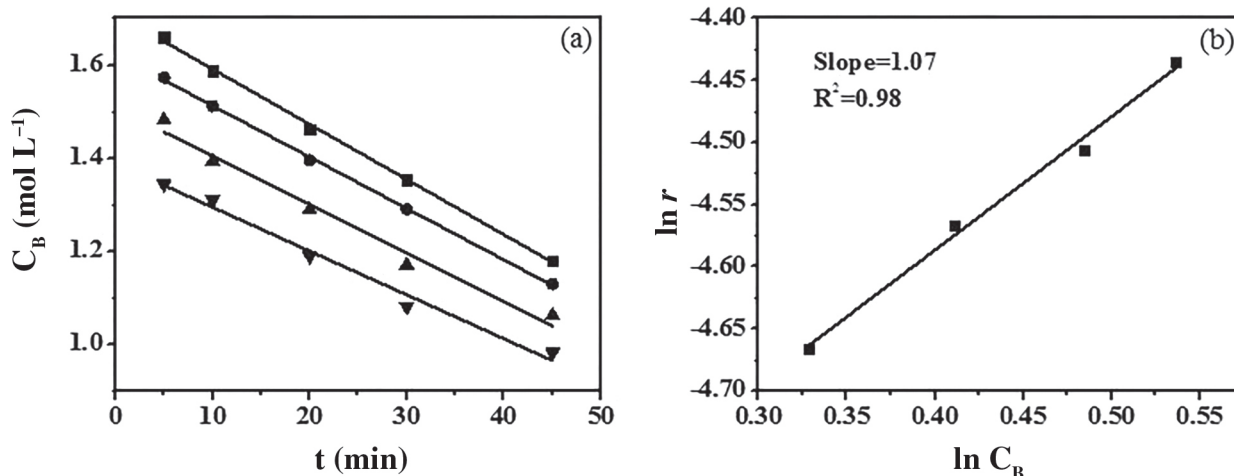


Figure 5. (a) Changes of H₂O₂ concentration (C_B) vs. time and (b) log-log plot of primary oxidation rate vs. initial C_B. Symbols for initial C_B values: (■) 2.08, (●) 1.93, (▲) 1.75, and (▼) 1.58 mol L⁻¹. Reaction conditions: catalyst amount, 9.90 g L⁻¹; BzH concentration, 0 mol L⁻¹; initial BzOH concentration, 1.28 mol L⁻¹; temperature, 393 K.

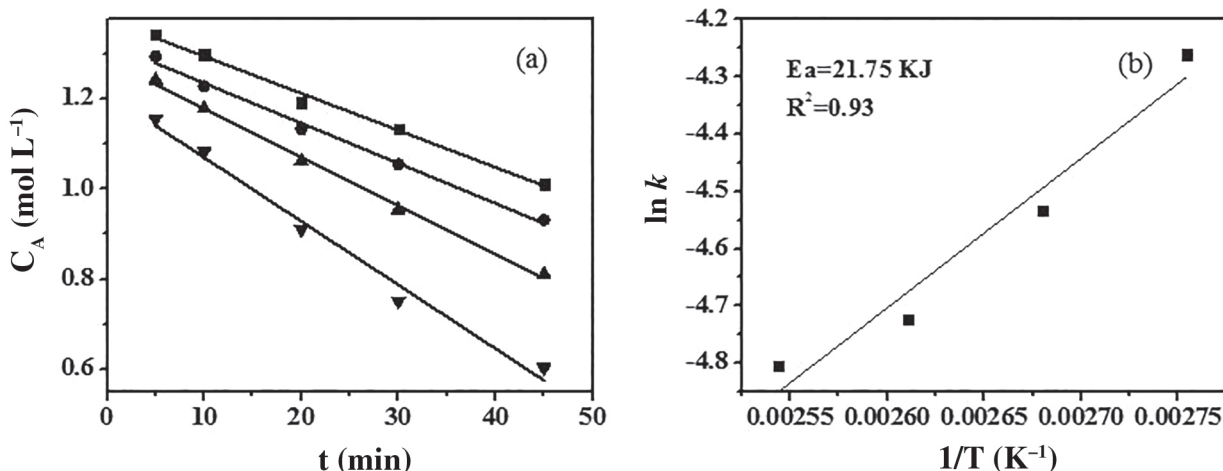


Figure 6. (a) Changes of BzOH concentration vs. time under various temperatures and (b) the corresponding Arrhenius plot. Symbols for different temperature: (■) 363, (●) 373, (▲) 383, and (▼) 393 K. Reaction conditions: catalyst amount 9.90 g L⁻¹; initial H₂O₂ concentration 2.08 mol L⁻¹ and BzOH concentration 1.67 mol L⁻¹.

[DMBPSH]H₂PW₁₂O₄₀ catalyst (36.18 kJ mol⁻¹),³⁷ and much less than that obtained over [PheH]H₂PW₁₂O₄₀ catalyst (56.7 kJ mol⁻¹) on the oxidation of BzOH to BzH with H₂O₂,³⁸ as well as oxidation of phenyl ethanol catalyzed by *N*-chlorinated *p*-toluenesulfonamide (*p*-TSA) salt (81.3 kJ mol⁻¹).⁶⁶ The results indicated that Sn_{1/2}H₂PW₁₂O₄₀ catalyst was a highly effective catalyst for the oxidation of BzOH with H₂O₂.

Conclusions

Transition-metal ion (M = Sn²⁺, Fe³⁺, Ni²⁺, Co²⁺, Ag⁺, Cu²⁺) exchanged TPA catalysts were favorably prepared and employed for the oxidation of BzOH with H₂O₂. The synergy effect of Brønsted-Lewis acid, strong Brønsted acidity, and pseudo-liquid characteristic of M-TPA catalysts positively affected catalytic activity.

Over these synthesized catalysts, the Sn_{1/2}H₂PW₁₂O₄₀ catalyst showed the best catalytic performances and was exploited in process optimization in order to acquire suitable conditions at catalyst amount of 5.5 wt.%, BzOH/H₂O₂ mole ratio of 1:1.25, 17 mL water amount and 3.3 h of reaction time. An excellent yield of BzH (95.1%) was obtained. These optimum experimental parameters were consistent with the RSM prediction on the basis of BBD model. According to the developed kinetic model, the reaction order was 2.64 and the E_a was 21.75 kJ mol⁻¹. Moreover, recyclability study had corroborated the effectiveness of Sn_{1/2}H₂PW₁₂O₄₀ catalyst and reproducibility for oxidation of alcohols.

Supplementary Information

Supplementary data (FTIR, XRD, TGA-DTG spectra,

contour plots and 3D response surface plots) are available free of charge at <http://jbcs.sbq.org.br> as PDF file.

Acknowledgments

The supports of this work by the National Key R&D Program of China (2018YFD0400600) and Jiangsu Key Laboratory of Regional Resource Exploitation and Medicinal Research (No. LPRK201701) are gratefully acknowledged.

Author Contributions

Yousheng Zhou was responsible for writing original draft; Xingyu Mei for the validation; Zhe Cai for the methodology and writing original draft; Qing Wang for the validation; Jiahui Duanmu for the methodology; Ouyang Kai for the data curation; Haijiang Zhang for the writing review and editing; Xiujuan Tang for the data curation; Xiaoxiang Han for the writing review and editing.

References

1. Parmeggiani, C.; Cardona, F.; *Green Chem.* **2012**, *14*, 547.
2. Mate, V. R.; Shirai, M.; Rode, C. V.; *Catal. Commun.* **2013**, *33*, 66.
3. Zhang, S.; Gao, S.; Xi, Z.; Xu, J.; *Catal. Commun.* **2007**, *8*, 531.
4. Yang, Z. W.; Zhao, X.; Li, T. J.; Chen, W. L.; Kang, Q. X.; Xu, X. Q.; Liang, X. X.; Feng, Y.; Duan, H. H.; Lei, Z. Q.; *Catal. Commun.* **2015**, *65*, 34.
5. Ma, L.; Jia, L. H.; Guo, X. F.; Xiang, L. J.; *Chin. J. Catal.* **2014**, *35*, 108.
6. Alabbad, S.; Adil, S. F.; Assal, M. E.; Khan, M.; Alwarthan, A.; Siddiqui, M. R. H.; *Arabian J. Chem.* **2014**, *7*, 1192.
7. Hosokawa, S.; Hosokawa, Y.; Imamura, S.; *Catal. Lett.* **2009**, *129*, 394.
8. Yang, X. M.; Wang, X. N.; Liang, C. H.; Su, W. G.; Wang, C.; Feng, Z. C.; Li, C.; Qiu, J. S.; *Catal. Commun.* **2008**, *9*, 2278.
9. Nasrollahzadeh, M.; Shafiei, N.; Nezafat, Z.; Bidgoli, N. S. S.; Soleimani, F.; *Carbohydr. Polym.* **2020**, *241*, 116353.
10. Nasrollahzadeh, M.; Shafiei, N.; Nezafat, Z.; Bidgoli, N. S. S.; *Mol. Catal.* **2020**, *489*, 110942.
11. Nasrollahzadeh, M.; Nezafat, Z.; Bidgoli, N. S. S.; Shafiei, N.; *Mol. Catal.* **2020**, *484*, 110775.
12. Shokouhimehr, M.; Yek, S. M. G.; Nasrollahzadeh, M.; Kim, A.; Varma, R. S.; *Appl. Sci.* **2019**, *9*, 4183.
13. Nasrollahzadeh, M.; Sajjadi, M.; Shokouhimehr, M.; Varma, R. S.; *Coord. Chem. Rev.* **2019**, *397*, 54.
14. Nasrollahzadeh, M.; Bagherzadeh, M.; Karimi, H.; *J. Colloid Interface Sci.* **2016**, *465*, 271.
15. Sudarsanam, P.; Malleshm, B.; Durgasri, D. N.; Reddy, B. M.; *J. Ind. Eng. Chem.* **2014**, *20*, 3115.
16. Corberán, V. C.; González-Pérez, M. E.; Martínez-González, S.; Gómez-Avilés, A.; *Appl. Catal., A* **2014**, *474*, 211.
17. Azam, K. D.; Babak, M.; Hamid, R. M.; *Fuel* **2019**, *236*, 717.
18. Xuan, N. P.; Tran, D. L.; Pham, T. D.; Nguyen, Q. M.; Thi, V. T. T.; Huan, D. V.; *Adv. Powder Technol.* **2018**, *29*, 58.
19. Peng, C.; Lu, X. H.; Ma, X. T.; Shen, Y.; Wei, C. C.; He, J.; Zhou, D.; Xia, Q. H.; *J. Mol. Catal. A: Chem.* **2016**, *423*, 393.
20. Choi, A. E. S.; Roces, S.; Dugos, N.; Wan, M. W.; *Sustainable Environ. Res.* **2016**, *26*, 184.
21. Yang, X. L.; Qiao, L. M.; Dai, W. L.; *Microporous Mesoporous Mater.* **2015**, *211*, 73.
22. Pamin, K.; Prończuk, M.; Basag, S.; Kubiak, W.; Sojka, Z.; Połtowicz, J.; *Inorg. Chem. Commun.* **2015**, *59*, 13.
23. Farsani, M. R.; Jalilian, F.; Yadollahi, B.; Rudbari, H. A.; *Polyhedron* **2014**, *76*, 102.
24. Leng, Y.; Zhao, P. P.; Zhang, M. J.; Wang, J.; *J. Mol. Catal. A: Chem.* **2012**, *358*, 67.
25. Zhao, W.; Zhang, Y. S.; Ma, B. C.; Ding, Y.; Qiu, W. Y.; *Catal. Commun.* **2010**, *11*, 527.
26. Tundo, P.; Romanelli, G. P.; Vázquez, P. G.; Aricò, F.; *Catal. Commun.* **2010**, *11*, 1181.
27. Zhou, Y.; Chen, G. J.; Long, Z. Y.; Wang, J.; *RSC Adv.* **2014**, *4*, 42092.
28. Misono, M.; *Catal. Today* **2009**, *144*, 285.
29. Han, X. X.; Kuang, Y. Y.; Ouyang, K.; Kan, R. J.; Tang, X. J.; Hung, C. T.; Liu, L. L.; Wu, P. H.; Liu, S. B.; *J. Taiwan Inst. Chem. Eng.* **2017**, *70*, 23.
30. Zhou, L.; Al-Zaini, E.; Adesina, A.; *Fuel* **2013**, *103*, 617.
31. Zhu, S. H.; Gao, X. Q.; Dong, F.; Zhu, Y. L.; Zheng, H. Y.; Li, Y. W.; *J. Catal.* **2013**, *306*, 155.
32. Pathan, S.; Patel, A.; *Appl. Catal., A* **2013**, *459*, 59.
33. Wang, S. S.; Zhang, J.; Zhou, C. L.; Vo-Thanh, G.; Liu, Y.; *Catal. Commun.* **2012**, *28*, 152.
34. Choi, J. H.; Kim, J. K.; Park, S.; Song, J. H.; Song, I. K.; *Appl. Catal., A* **2012**, *427-428*, 79.
35. Kozhevnikov, I. V.; *Chem. Rev.* **1998**, *98*, 171.
36. Essayem, N.; Holmqvist, A.; Gayraud, P. Y.; Vedrine, J. C.; Taarit, Y. B.; *J. Catal.* **2001**, *197*, 273.
37. Ouyang, K.; Han, X. X.; Xiong, C. H.; Tang, X. J.; Chen, Q.; *Green Process. Synth.* **2017**, *6*, 385.
38. Han, X. X.; Kuang, Y. Y.; Xiong, C. H.; Tang, X. J.; Chen, Q.; Hung, C. T.; Liu, L. L.; Liu, S. B.; *Korean J. Chem. Eng.* **2017**, *34*, 1914.
39. Sun, Z.; Wang, S. T.; Wang, X. H.; Jiang, Z. J.; *Fuel* **2016**, *164*, 262.
40. Han, X. X.; Chen, K. K.; Yan, W.; Hung, C. T.; Liu, L. L.; Wu, P. H.; Lin, K. C.; Liu, S. B.; *Fuel* **2016**, *165*, 115.
41. Han, X. X.; Yan, W.; Chen, K. K.; Hung, C. T.; Liu, L. L.; Wu, P. H.; Huang, S. J.; Liu, S. B.; *Appl. Catal., A* **2014**, *485*, 149.

42. Han, X. X.; He, Y. F.; Hung, C. T.; Liu, L. L.; Huang, S. J.; Liu, S. B.; *Chem. Eng. Sci.* **2013**, *104*, 64.
43. Ding, Y.; Zhao, W.; *J. Mol. Catal. A: Chem.* **2011**, *337*, 45.
44. Afzalnia, A.; Mirzaie, A.; Nikseresht, A.; Musabeygi, T.; *Ultrason. Sonochem.* **2017**, *34*, 713.
45. Qin, L. B.; Zheng, Y.; Li, D. Q.; Zhou, Y. S.; Zhang, L. J.; *Fuel* **2016**, *181*, 827.
46. Dong, X. B.; Wang, D. J.; Li, K. B.; Zhen, Y. Z.; Hu, H. M.; Xue, G. L.; *Mater. Res. Bull.* **2014**, *57*, 210.
47. Zhao, H. H.; Zeng, L. X.; Li, Y. L.; Liu, C.; Hou, B.; Wu, D.; Feng, N.; Zheng, A. M.; Xie, X. L.; Su, S. P.; Yu, N. Y.; *Microporous Mesoporous Mater.* **2013**, *172*, 67.
48. Izumi, Y.; Urabe, K.; *Chem. Lett.* **1981**, *10*, 663.
49. Zheng, A.; Li, S.; Liu, S. B.; Deng, F.; *Acc. Chem. Res.* **2016**, *49*, 655.
50. Zheng, A.; Huang, S. J.; Liu, S. B.; Deng, F.; *Phys. Chem. Chem. Phys.* **2011**, *13*, 14889.
51. Huang, S. J.; Yang, C. Y.; Zheng, A.; Feng, N.; Yu, N.; Wu, P. H.; Chang, Y. C.; Lin, Y. C.; Deng, F.; Liu, S. B.; *Chem. - Asian J.* **2011**, *6*, 137.
52. Zheng, A.; Huang, S. J.; Chen, W. H.; Wu, P. H.; Zhang, H.; Lee, H. K.; de M nerval, L. C.; Deng, F.; Liu, S. B.; *J. Phys. Chem. A* **2008**, *112*, 7349.
53. Hu, C.; He, Q.; Zhang, Y. H.; Liu, Y.; Zhang, Y. F.; Tang, T.; Zhang, J.; Wang, E.; *Chem. Commun.* **1996**, *27*, 121.
54. da Silva, M. J.; Liberto, N. A.; Lorena, C. D. A. L.; Pereira, U. A.; *J. Mol. Catal. A: Chem.* **2016**, *422*, 69.
55. da Silva, M. J.; Julio, A. A.; Ferreira, S. O.; da Silva, R. C.; Chaves, D. M.; *Fuel* **2019**, *254*, 115607.
56. Li, L. X.; Liu, B. Y.; Wu, Z. W.; Yuan, X.; Luo, H.; *Chem. Eng. J.* **2015**, *280*, 670.
57. Chu, Y. Y.; Yu, Z. W.; Zheng, A.; Fang, H. J.; Zhang, H. L.; Huang, S. J.; Liu, S. B.; Deng, F.; *J. Phys. Chem. C* **2011**, *115*, 7660.
58. Gui, J. Z.; Liu, D.; Sun, Z. L.; Liu, D. S.; Min, D. Y.; Song, B. S.; Peng, X. L.; *J. Mol. Catal. A: Chem.* **2010**, *331*, 64.
59. Kumar, R. Ch.; Rao, K. T. V.; Prasad, P. S. S.; Lingaiah, N.; *J. Mol. Catal. A: Chem.* **2011**, *337*, 17.
60. Ahmad, J. U.; R is nen, M. T.; Leskel , M.; Repo, T.; *Appl. Catal., A* **2012**, *411-412*, 180.
61. Chevallier, M. L.; Dessolin, S.; Serres, F.; Bruyas, L.; Chatel, G.; *Molecules* **2019**, *24*, 4157.
62. Bongiorno, A.; Landman, U.; *Phys. Rev. Lett.* **2005**, *95*, 106102.
63. Pozdnyakova-Tellinger, O.; Teschner, D.; Kr hnert, J.; Jentoft, F. C.; Knop-Gericke, A.; Schl gl, R.; Wootsch, A.; *J. Phys. Chem. C* **2007**, *111*, 5426.
64. Teschner, D.; Wootsch, A.; Pozdnyakova-Tellinger, O.; Kr hnert, J.; Vass, E. M.; H vecker, M.; Zafeiratos, S.; Schn rch, P.; Jentoft, P. C.; Knop-Gericke, A.; Schl gl, R.; *J. Catal.* **2007**, *249*, 318.
65. Whitcomb, P. J.; Helseth, T.; *Design-Expert 6.0.5*; Stat-Ease, Inc., USA, 2001.
66. Ramachandra, H.; Rangappa, K. S.; Mahadevappa, D. S.; Made Gowda, N. M.; *Monatsh. Chem.* **1996**, *127*, 241.

Submitted: April 20, 2020

Published online: August 14, 2020

